BULK NANOCOMPOSITES PRODUCED BY THERMALLY ACTIVATED SEVERE PLASTIC DEFORMATION

S. Zhang, J. Bai, K. Shue
M3TechCenter LLC,
Canton, MI 48188

X. Wu and Y. Liu
Department of Mechanical Engineering, Wayne State University,
Detroit, MI 48202

L. Dauerman
Department of Chemistry, New Jersey Institute of Technology,
Newark, NJ 07102

J. Mabesa Jr.
U.S. Army Tank-Automotive Command (TACOM),
Warren, MI 48397-5000

ABSTRACT

In this paper, several versions of extrusion processes were used to provide severe plastic deformation for grain refinement (with a modified ECAE extrusion) and for grain/fiber alignment (with straight extrusion). The process was performed at elevated temperatures to reduce extrusion pressure, and in order to increase strength and avoid grain growth secondary phases were added or in-situ formed. In addition, this study also attempt to develop a one-step material synthesis and net-shape forming technique for shape memory alloys, which starts at elementary metals and the chemical reaction synthesis was triggered at a low temperature (400-600 C) and with sustained reaction. The generated heat was used for compression or extrusion to form desired final components at improved properties. The produced materials were characterized by optical microscopy (OM), scanning electron microscopy (SEM) and transmission electron microscopy (TEM).

In order to understand the process and microstructure alignment, several modeling methods were used, including analytical and finite element methods. The potential for extending this process for manufacturing smart materials with improved performances, such as shape memory effect of nano-grained shape memory alloys in many MEMS and sensor applications, is also discussed.

1. INTRODUCTION

For many structural applications such as automotive and aerospace structural components, a high specific strength of material is critical. Among many other approaches for material strengthening, development of super-fine-and nano-grained microstructure and with nano-grain composite is of current interest. In recent years extensive effort has been made in developing bulk nano materials by severe plastic deformation, such as equal channel angular extrusion (ECAE) (Segal 1995, 1999, 2004), in which materials with a regular grain size can be break down to super-fine-grained microstructure by simple shear deformation with a mean grain size ranging from ten nanometers to submicron scale in about five extrusion passes. One of the current concerns on mass production of this high-efficiency ECAE process is the limitation of material's ductility, which causes fracture both during and after severe plastic deformation.

This study attempts to develop a thermally activated ECAE process for producing nano-composites that is either in-situ developed or artificially tailored. Although ECAE process at warm or elevated temperatures has been reported for some alloys such as magnesium alloys due to the fact that only by heating the process can be performed without pronounced fracture development, the heating causes significant grain growth and limits the grain refinement. The second phase can play the role as a grain growth prohibitor.

The application of ECAE process in shape memory materials is also of current interest, due to high demands in MEMS and miniaturization of Microsystems and actuators. Traditional SMA manufacturing route is to synthesis shape memory alloy by chemical metallurgy to produce cast ingot; then the ingots are reheated to elevated temperature, and form homogenous cross sections such as bars, rods, wires and tubes etc. Due to the poor ductility of this class of intermetallics at room temperature, shaping by plastic deformation or machining is difficult and costly, requiring reheating again to elevated temperatures (~1000ºC). Reaction synthesis has been developed for porous SMA (Chu et al. 1997; Chung et al. 2004; Kim et al. 2004), for

Report Documentation Page

Form Approved
OMB No. 0704-0188

1. REPORT DATE	2. REPORT TYPE	3. DATES COVERED
DEC 2008	**N/A**	**-**

4. TITLE AND SUBTITLE	5a. CONTRACT NUMBER
Bulk Nanocomposites Produced By Thermally Activated Severe Plastic Deformation	5b. GRANT NUMBER
	5c. PROGRAM ELEMENT NUMBER
6. AUTHOR(S)	5d. PROJECT NUMBER
	5e. TASK NUMBER
	5f. WORK UNIT NUMBER
7. PERFORMING ORGANIZATION NAME(S) AND ADDRESS(ES) **M3TechCenter LLC, Canton, MI 48188**	8. PERFORMING ORGANIZATION REPORT NUMBER
9. SPONSORING/MONITORING AGENCY NAME(S) AND ADDRESS(ES)	10. SPONSOR/MONITOR'S ACRONYM(S)
	11. SPONSOR/MONITOR'S REPORT NUMBER(S)

12. DISTRIBUTION/AVAILABILITY STATEMENT
Approved for public release, distribution unlimited

13. SUPPLEMENTARY NOTES
See also ADM002187. Proceedings of the Army Science Conference (26th) Held in Orlando, Florida on 1-4 December 2008, The original document contains color images.

14. ABSTRACT

15. SUBJECT TERMS

16. SECURITY CLASSIFICATION OF:			17. LIMITATION OF ABSTRACT	18. NUMBER OF PAGES	19a. NAME OF RESPONSIBLE PERSON
a. REPORT	b. ABSTRACT	c. THIS PAGE			
unclassified	**unclassified**	**unclassified**	**UU**	**8**	

some medical application. One work by (Locci et al. 2003) used current and pressure to activate the reaction synthesis and resulted in dense NiTi with some secondary phases.

In this paper a feasibility study is provided to explore the possibility of a new SMA manufacturing route: the process starts from raw material powders that are the basic elements required for synthesis shape memory alloys. Controlled by thermodynamics and kinetics of the solid-state chemical reaction, the heat generated from the reaction is sufficient to sustain the reaction, so that the synthesis reaction can be started by ignition from one end of the compact at a very low temperature (~400ºC), and self-propagated to entire powder compact, with the ending temperature being above 1000ºC.

2. EXPERIMENTAL AND MODELING CONDITIONS

2.1 Materials and Mechanical Mixing of Powders

The raw materials used in this study include: powders of aluminum alloys AA6061, Ni, Ti, Carbon Nanotubes (CNT), and aluminum oxides (mean particle size at 50nm)

The AA6061-CNT was processed in the following procedures: the two constituents were mixed at 99.5:0.5 weight ratios, and then attrition milled in methanol with aluminum oxide balls at 3mm in diameter, for 4 hrs for reducing initial powder diameter. The resulting slurry was ultrasonically vibrated for 2 hour inside a high power ultrasonic cleaner combined with heating at 60 C, in order to disperse CNT. At the end of the process dried powders were obtained.

Similar process was used for mixing Ni-Ti at 50:50 molar ratio, or with additional 5w% addition of nano aluminum oxide powder Al_2O_3 (at a mean powder size of 50nm). These prepared powders were cold pressed into billets of 10mm in diameter and various heights, depending on the extrusion process used.

2.2 Modified Equal Channel Angular Extrusion And Straight Extrusion

For grain refinement and further mixing by severe plastic deformation, a modified ECAE process was used. In this process half of the outlet rod in cross-sectional area was used, in order to achieve 2:1 area reduction yet permit two halves to combine into a full billet for repeated extrusion. We call this process Half-Channel Angular Extrusion (HCAE). Due to very high extrusion force in this process, the extrusion was performed at 450 C-550°C for AA6061-CNT. In order to improve CNT alignment, after ECAE, a straight extrusion at the extrusion ratio of 4:1 to 9:1 was used that is equivalent to an additional extrusion true strain of 1.4 or 2.2 (or engineering strain of 300% and 800%), respectively.

For NiTi extrusion, Ni-50at%Ti billet was placed inside a thick-wall tube (die) with OD=60 mm and ID=10 mm. an induction coil was placed surrounding the die, and the temperature was controlled with a programmable temperature controller. The ECAE and straight extrusion setups are shown in Fig 1. In addition, in order to get the reaction synthesize temperature under the current condition, a separate set of experiments were performed without tools, so that the billet was exposed, allowing the reaction temperature to be measured by an IR non-contact temperature sensor. Direct current was used to heat up a wire as a means of trigger to initiate self-sustained chemical reaction. A wire is powered and resistively heated by a DC power supply, which can provide up to 100 A current. In this test, 18A DC current was used to heat the wire to red-hot and to provide the ignition. The NiTi billet came into self combustion when being ignited. During the reaction synthesis a video movie was made, and an infrared temperature sensor was used to record the temperature.

Separate experiment was performed that repeated the above mentioned reaction synthesis first and then, when the reaction zone swept through entire sample, a hot forging process started, to compress the sample into a full density. Depending on the die geometry the final shape can be a flat disk, a cup, or a 3D component. If the process is performed inside an extrusion chamber, after reaction and temperature rising the in-situ densification and extrusion deformation can be followed. A large plastic deformation is helpful in obtaining better microstructure.

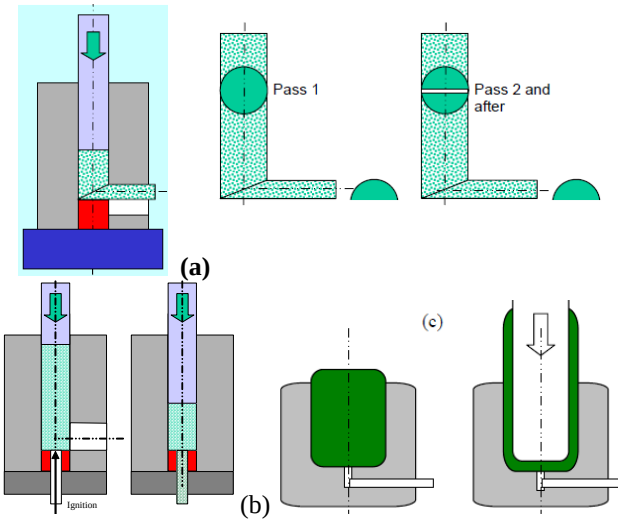

Fig. 1. Schematic of modified ECAE process for grain refinement (a), followed by straight extrusion for grain/reinforcement alignment (b), or reverse extrusion for forming a cup (for shape memory fasteners).

2.3 Combined Reaction Synthesis And Forming

To take all advantages of various material processing methods, we may combine the reaction synthesis with different forming processes for specific component manufacturing depending on the applications. Figure 2 shows several possibilities of the process. For ECAE process furnace reheating is needed in the 2nd pass and after. These processes not only reduce energy consumption by using reaction heat release for elevated temperature forming and allow theoretical density and homogeneous material chemical/mechanical properties; it can adopt several material reinforcement methods, such as addition nano-reinforcements (including Carbon Nanotubes), microstructural refinement and alignment, and net-shape forming to 3D geometry.

3. EXPERIMENTAL RESULTS

With the modified ECAE process or HCAE that gives an area reduction of 2, the AA6061 powder with 5w% CNT can be extruded at a temperature ranging 450-550 C. Samples are shown in Fig 3. The TEM result on the products is shown in Fig 4. It can be seen that a good interface adhesion was developed between CNT and Al, due to the high temperature and high pressure process. This allows realization of CNT reinforcement. Due to very high CNT loading (5w%, for the purpose of enhancing thermal and electrical conductivity), CNT agglomerations are seen in many locations.

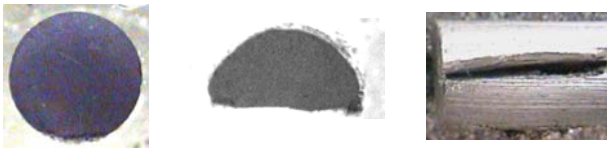

Initial Pass-1 Pass-1

Fig. 2. Samples from HCAE process

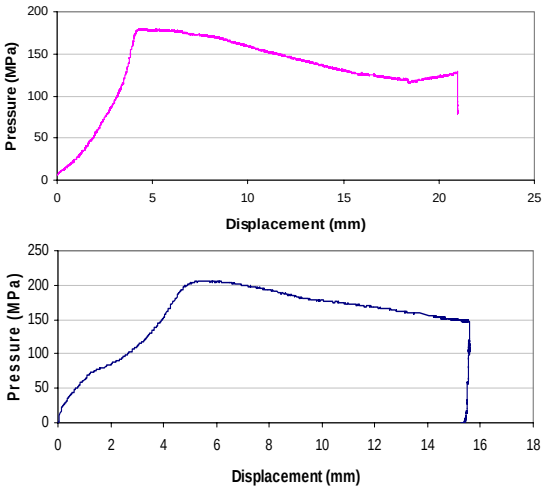

Fig. 3. Load-displacement curves of HCAE in the first and second passes.

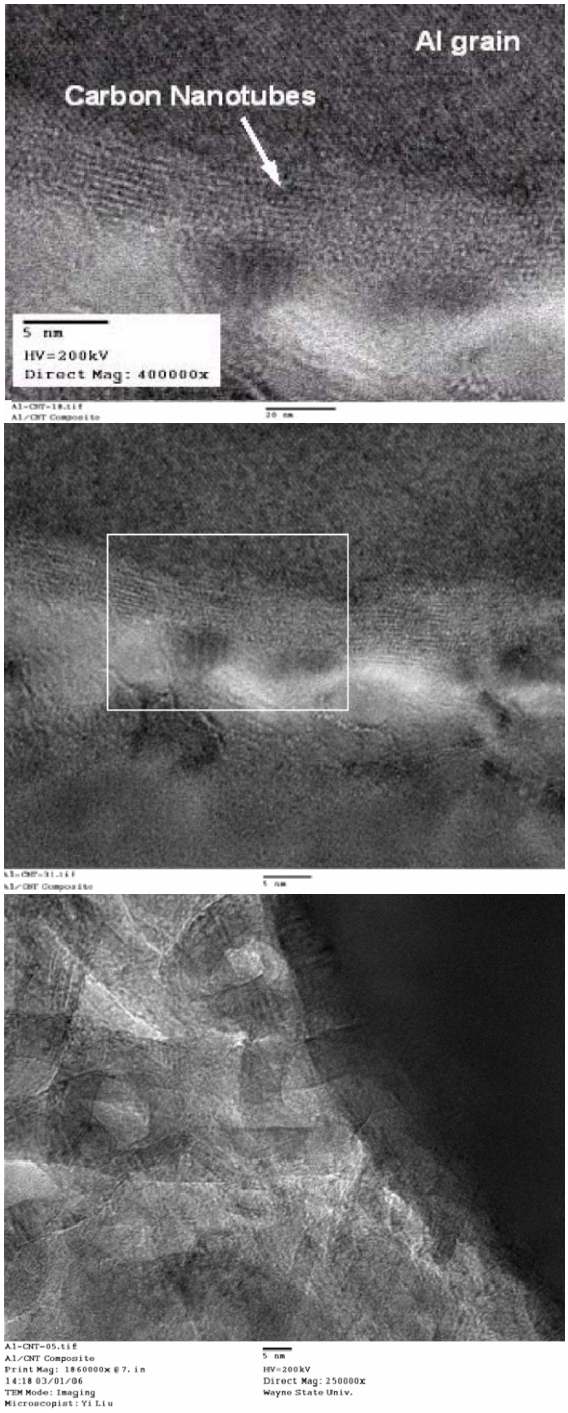

Fig. 4. The bright-field images of transmission electron microscope showing the formation of the tangled CNTs and the formation of CNT-Al strong bonding. The top is the local enlargement in the boxed area, and the bottom shows CNT agglomeration.

In order to further provide fiber alignment, straight extrusion was performed also at the same temperature range. Fig 5 shows samples extruded with extrusion ratios

of R=4 and 9, respectively. The load-displacement curves at R=9 is shown. At the early stage of the process there is a filling process to eliminate any clearance/cavities between the billet and the extrusion chamber. After that the load is raising and reaches a peak value, and then it decreases with reduction of remaining billet length, an effect of friction on the extrusion force. At the very end of the process the load increases again due to the effect of dead end.

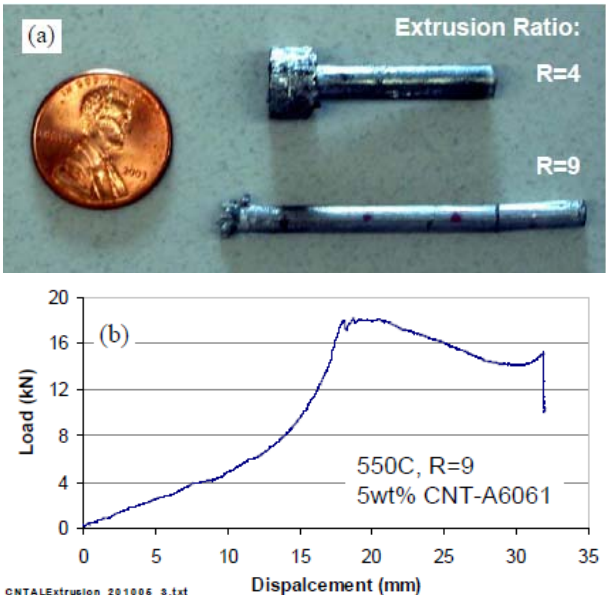

Fig. 5. Straight extrusion of CNT-AA6061 composite at 550ºC.

For developing a one-step combined shape memory synthesis and net-shape forming, the reaction synthesis was studied. Figure 6 shows the temperature vs. time of the billet during reaction synthesize, and the selected images at the corresponding time indicated in the plot. The reaction took place in only about 3 seconds when the flame swept the entire sample. After that the sample remained red-hot temperature for about 20 seconds, and then it turned into dark and further cooling down to room temperature. The product of this process is a porous and strong billet with slightly reduced dimension. The reaction synthesis process generates large amount of heat that makes the sample to be at over 1000 C, ideal for further plastic deformation to make net-shape components in one step. Thus, a follow-up deformation process was added to achieve full theoretical density and a desired shape.

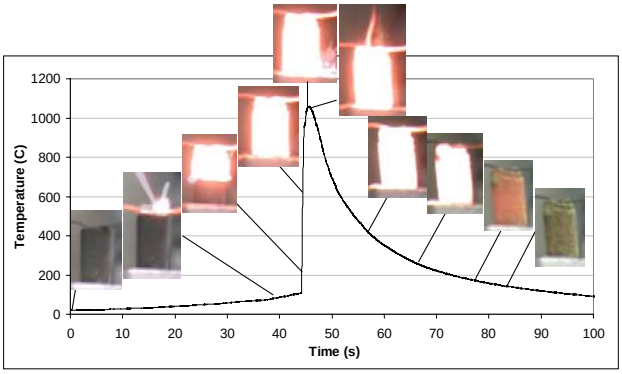

Fig. 6. Temperature vs. time during reaction synthesize of NiTi shape memory alloy from powders of Ni and Ti at 50:50 molar ratio. The reaction completed in about 3 seconds, and the peak temperature was over 1000ºC. The billet size (powder compact) is 10-mm diameter and 20-mm height.

A sample from the one-step process with reaction synthesis and instant compression was shown in Fig 7. It shows nearly fully density as compared with most published works with high porosities from self-sustained reaction synthesis.

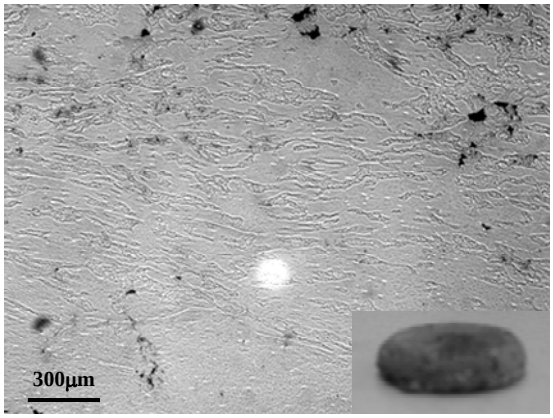

Fig. 7. Microstructure of a sample from combined synthesize and in-situ compression. The inset is the photo of the billet with the diameter about 20 mm and height is 3 mm that was compressed from the billet size of 12-mm diameter and10-mm height.

X-ray diffraction patterns were measured, on the products from self-sustained reaction synthesis, see Fig 8. By indexing all the peaks, it is found that majority powders have turned into NiTi intermetallic in the form of martensite phase, and some NiTi2 was also forms, probably due to local chemical fluctuation. Since the product thus formed contains multiple phases, the microstructure is stable. In addition, small amount of residual metal Ni and Ti remains that can be further improved by through mixing process.

The NiTi with 5w% Al2O3 nano particles were also processed, but the resulting XRD peaks obtained is the same as that without it, due to weak signals from the analysis.

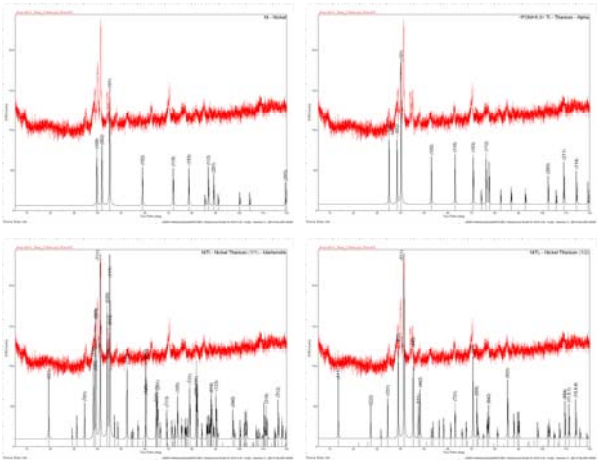

Fig. 8. XRD with index for NiTi, showing

4. MODELING

The modeling of the extrusion process is for better understanding the energy dissipation and fiber alignment (for CNTs) during the extrusion process, for better process design. Two methods were used for the mechanical analyses, i.e. Analytical method with upper bound, and FEA method.

4.1 Extrusion Analysis

The first method used an upper bound analytical approach (Hosford; Caddell 1993). The simplified velocity field for the ECAE is shown in Fig 9.

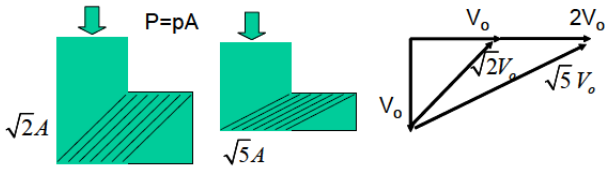

Fig. 9. Velocity field used for upper bound analysis of ECAE process

Based on this flow field, for ECAE: Rod of diameter D, or Rectangular bar of section (a x b):

$$p/2k = 1 + 2(1.1)mL/D \quad (1)$$

where

D = rod diameter or mean side length, 1/D=1/a + 1/b,

m = 0~1, (the frictional stress = mk),

For Half Channel Angular Extrusion (HCAE): similarly

$$p/2k = 2.5 + 2mL/D \quad (2)$$

The calculated results for half channel and equal channel 90º angular extrusion into a round bar are shown in Fig. 10. The values for billet length of zero (shown at the very right-end of the figure) reflect the net extrusion pressure associated with 90º shear at the cross-channel section,

For pure shear this gives p/2k=1 if there is no reduction in cross-sectional area, and equals to 2.5 for extrusion ratio of 2. The increase in extrusion pressure with the length of the inlet billet reflects the effect of chamber-workpiece friction, which increases significantly based on dry friction. This term actually dominates the total extrusion pressure or force of the process. This analysis clearly indicates that lubrication at the tool-workpiece contact interface is critical for the success of the process.

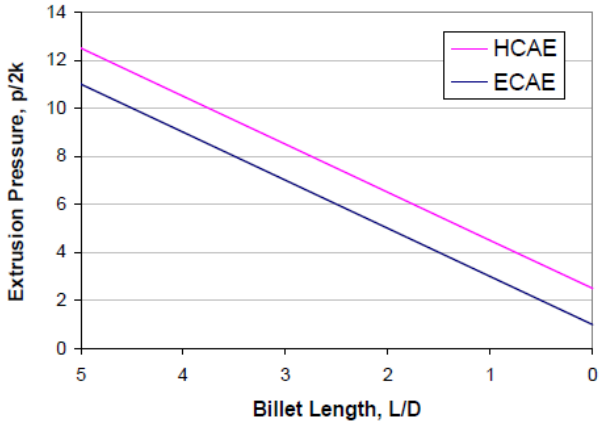

Fig. 10. Computed extrusion pressure as a function of length-to-diameter ratio of the billet, for Half-Channel and Equal-channel extrusion.

For straight extrusion with a conical die, the simplified velocity field is shown in Fig 11a. In this analysis, The material deformation resistance Y* obeys a power-law strain rate hardening equation, and the strain rate changes over the axial coordinate x or diameter D, with the inlet velocity and diameter to be Vi and Di

$$Y^* = k\dot{\varepsilon}^m = k(V_i / D_i)^m \quad (3)$$

With the consideration of the effects of temperature and grain size on the flow stress, the pre-factor k here is given by

$$k = k_o \exp\left(\frac{mQ}{RT}\right)\left(\frac{d}{d_0}\right)^m \quad (4)$$

The strain-enhanced dynamic grain growth or grain refinement can be expressed by a power-law relationship

$$d = d_0^{\lambda\varepsilon} \quad (5)$$

And the static grain growth due to heating for time t results the grain size of

$$F_d = (1+\alpha t)^{mp/q} \tag{6}$$

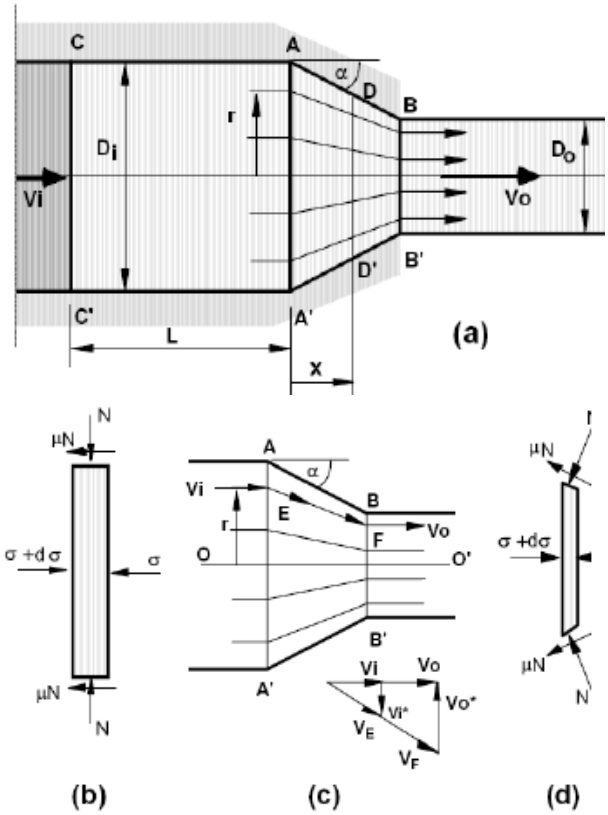

Fig. 11. Deformation geometry and material flow, used for the analysis of (a) extrusion flow line of homogeneous deformation; (b) a slab element between AA' and CC; (c) velocity discontinuity at AA' and BB'; (d) a slab element between AA' and BB'.(Hosford; Caddell 1993; Wu; Chen 1992)

The extrusion force from within the conical die is given by the slab force balance plus the effect of velocity discontinuity at the inlet and outlet vertical sections,

$$F_g = (4\tan\alpha)^m \left\{ \frac{1+B}{B+1.5m+\lambda mp}\left(R^{B+1.5m+\lambda m}-1\right) + \frac{\tan\alpha}{3}\left(R^{1.5m+\lambda m}+1\right)\right\} \tag{7}$$

where R is the extrusion ratio, B=μ/tanα

The friction force between the chamber and the billet before entering the conical die provides additional contribution over the extrusion force Fg.

$$F_f = \exp(\mu L / D_i) \tag{8}$$

The total extrusion force P consists of 4 terms related to material intrinsic flow stress at a reference strain Y* , the extrusion geometry factor Fg, the grain size effect Fd considering conventional microstructural evolution due to grain growth (static and dynamic) and gain refinement, and the friction from the extrusion container Ff, that is

$$P = Y^* \cdot F_g \cdot F_d \cdot F_f \tag{9}$$

This is the final model for straight extrusion at elevated temperatures.

The second method for the process analysis is based on FEA with Abaqus source code. The equivalent strain distribution during ECAE is shown in Fig 12.

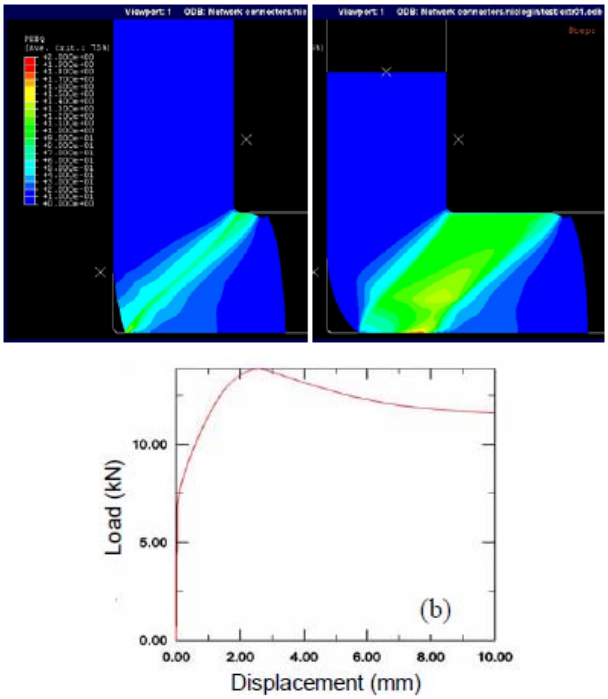

Fig. 12. Effective strain distribution at two moments of the extrusion (a), and load vs. displacement (b) in ECAE for AA6061 at RT, from Abaqus FEA simulation.

4.2 Modeling Fiber Alignment In Straight Extrusion

A geometrical model was developed for describing the evolution of a fiber rotation within a deformation field. For an initially random distribution of fibers, the probability for a fiber to be oriented within an angle ϕ can be accounted for as the ratio of the surface area of a crown extended from the pole to the angle ϕ, over the area of the hemispherical dome. See Fig 13. Thus,

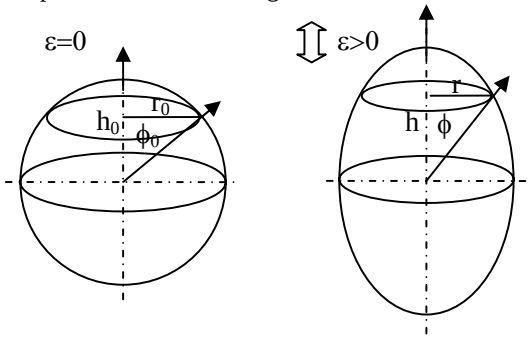

Fig. 13. The schematic demonstration of a fiber rotated from initial orientation angle ϕ_0 to ϕ after axial strain ε.

$$F(\phi) = 1 - \cos\phi \quad (0 \le \phi \le \pi/2) \tag{10}$$

The orientation distribution function (ODF) is the differentiation of F

$$f(\phi) = \frac{dF(\phi)}{d\phi} = \sin\phi \tag{11}$$

For a sphere with a fiber originally oriented at $\tilde{\phi}$ from the north pole, after a tensile stretch strain of ε, will rotate to ϕ. From geometrical relationship we have

$$\frac{\tan\phi}{\tan\phi_0} = \frac{r}{h} \Big/ \frac{r_0}{h_0} = \exp(-\varepsilon)\cdot\exp(-0.5\varepsilon) = \exp(-0.5\varepsilon) \tag{11}$$

or,

$$\phi_0 = \tan^{-1}\left[\exp(1.5\varepsilon)\tan\phi\right] \tag{13}$$

$$\varepsilon = \ln(R) \tag{14}$$

Note that the probability of a fiber aligned within $\tilde{\phi}$ at ε=0 is the same as that within ϕ after a strain ε,

$$F(\phi,\varepsilon) = F_0(\phi_0) = 1 - \cos\left\{\tan^{-1}\left[\exp(1.5\varepsilon)\tan\phi\right]\right\} \tag{15}$$

$$F(\phi,\varepsilon) = 1 - \left\{1 + \tan^2\phi\exp(3\varepsilon)\right\}^{-0.5} \tag{16}$$

Thus, the ODF as a function of strain is

$$f(\phi,\varepsilon) = \frac{\partial}{\partial\phi}F(\phi,\varepsilon) = \exp(3\varepsilon)\left\{1 + \tan^2\phi\exp(3\varepsilon)\right\}^{-1.5}\cdot\tan\phi\cdot\sec^2\phi \tag{17}$$

To apply this simple geometrical fiber rotation model to an extrusion case, with the assumption that the deformation is uniform across the radius, the strain in the axial direction is related to the extrusion area reduction R simply by

$$R = \frac{A_0}{A} = \frac{L}{L_0} = exp(\varepsilon), \text{or} \quad \varepsilon = ln(R) \tag{18}$$

It is also necessary to obtain the 2D distribution function over the sectioned plane that is parallel to the extrusion direction, so that the microstructural alignment can be experimentally realized. For the 2D section along the extrusion direction, a similar derivation can be performed with the initial fiber orientation angle $\tilde{\varphi}$ to be randomly distributed, or the probability density to be homogeneous over 0~π/2 range,

$$g_0(\varphi_0) = 2/\pi \quad (0 \le \varphi_0 \le \pi/2) \tag{19}$$

By integration, the measured fiber orientation within $\tilde{\varphi}$ is

$$G_0(\varphi_0) = 2\varphi_0/\pi \quad (0 \le \varphi_0 \le \pi/2) \tag{20}$$

After 1D straining . in the extrusion direction,

$$G(\varphi,\varepsilon) = G_0(\varphi_0) = \frac{2}{\pi}\tan^{-1}\left(\exp(1.5\varepsilon)\tan\varphi\right) \quad (0 \le \varphi \le \frac{2}{\pi}) \tag{21}$$

And by differentiating G with respect to φ, the fiber orientation density distribution is obtained,

$$g(\varphi,\varepsilon) = \frac{2}{\pi}\exp(1.5\varepsilon)\left\{\cos^2\varphi + \sin^2\varphi\exp(3\varepsilon)\right\}^{-1} \tag{22}$$

The fiber orientation distribution over 3D solid angle ϕ and its 2D projection φ over a section parallel to the extrusion axis are plotted in Fig 14a, b respectively as a function of extrusion ratio R. It can be seen that with extrusion ratio of 4 and 9 (or the die diameter ratio of 2 and 3) the fiber orientation effect can be so strong.

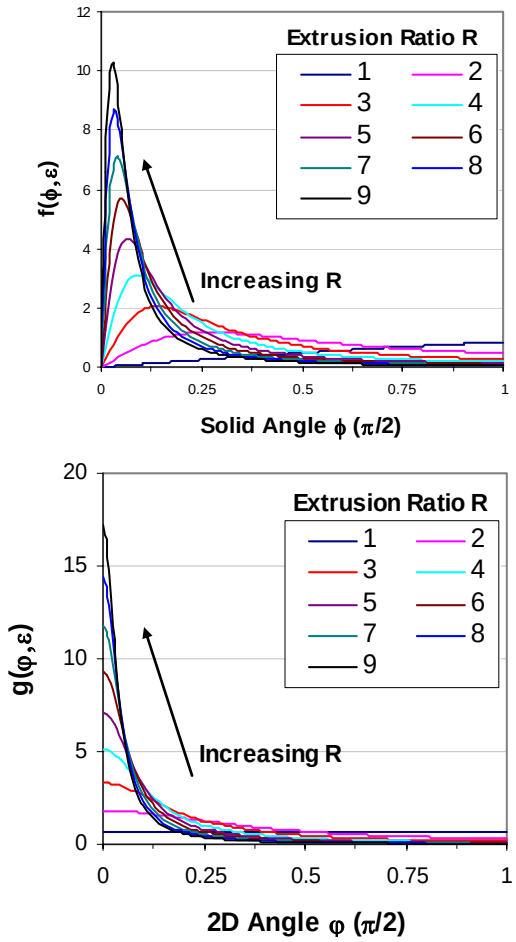

Fig. 14. The predicted fiber orientation distribution density for various extrusion ratios, in 3D space (top) and 2D sectioned surface (bottom), where angle 0 is at the extrusion axis showing.

5. DISCUSSION

5.1 The Problems Related To The Observed Results

To further improve the severe deformation process, several problems are to be resolved, they are:

Incomplete bonding of two halves of extruded bars may form when the extrusion speed is too high, or temperature is too low, or when the connecting surface of the two halves is contaminated (here the used BN powders

as solid lubricant was used, but it had great chance getting between the two halves before extrusion and avoided pressure/deformation assisted diffusion bonding process)

.

Edge cracking caused by non-uniform deformation: ECAE extrusion gets the best effect of uniform deformation for squared bar section. Current section of half round does not assure uniform shear across the cross-sectional area caused non-uniform shear. The use of half-section billet makes the deformation even more non-uniform.

Not uniform distribution of CNT within matrix: The reasons are two folds: a) there still need to improve original CNT dispersion within liquid suspension stage; During cold and high temperature compaction it needs to avoid re-agglomeration; (b) refining grain size of aluminum matrix. Due to much larger initial Al powder size CNTs stayed in the pockets of aluminum powders, so that even original CNTs were dispersed (we believe this is the case since CNT suspension was not settled over week-long period).

5.2 Configuration Of Combined Reaction Synthesis And Forming

To take all the advantages of various material processing methods, we may combine the reaction synthesis with different forming processes for specific component manufacturing depending on the applications. Figure 15 shows several possibilities of the process. For ECAE process furnace reheating is needed in the 2nd pass and after. These processes not only reduce energy consumption by using reaction heat release for elevated temperature forming and allow theoretical density and homogeneous material chemical/mechanical properties; it can adopt several material reinforcement methods, such as addition nano-reinforcements (including carbon nanotubes), microstructural refinement and alignment, and net-shape forming to 3D geometry.

6. CONCLUSIONS

Experimental study is provided on a modified ECAE process, which provides opportunities to repeat the extrusion ratio of 2 in each pass and is capable of accumulating severe plastic deformation. The extrusion was performed at elevated temperatures to reduce extrusion pressure and increase in material's ductility to avoid cracking. To enhance material strength and possibly other physical properties, nano-reinforcements were added at powder stage.

We have developed fundamental understandings on the mechanisms involved in the above mentioned material processes, along with phenomenological models. These models are: (1) Extrusion model: for both straight extrusion and angular extrusion; (2) Alignment model for inclusions (including carbon nanotubes) during plastic deformation; (3) Constitutive model (including strain recovery behavior) of shape memory polymers as a function of Tg temperature and molecular size distribution, capable of simulating hysteresis loop for material design with improved reliability. These new concepts and new understandings provide significant advancement in the area of smart material processing and application.

ACKNOWLEDGEMENT

Funding support of this study is provided by US Army under Contract W56HZV08C0303.

REFERENCES

Chu, C. L., B. Li, S. D. Wang, S. G. Zhang, X. X. Yang, and Z. D. Yin, 1997: Preparation of TiNi shape memory alloy porosint by SHS. *Transactions of Nonferrous Metals Society of China*, **7,** 84-87.

Chung, C. Y., C. L. Chu, and S. D. Wang, 2004: Porous TiNi shape memory alloy with high strength fabricated by self-propagating high-temperature synthesis. *Materials Letters*, **58,** 1683-1686.

Hosford, W. F., and R. M. Caddell, 1993: *Metal Forming (2nd edition)*. Prentice-Hall, Inc.

Kim, J. S., J. H. Kang, S. B. Kang, K. S. Yoon, and Y. S. Kwon, 2004: Porous TiNi biomaterial by self-propagating high-temperature synthesis. *Advanced Engineering Materials*, **6,** 403-406.

Locci, A. M., R. Orru, G. Cao, and Z. A. Munir, 2003: Field-activated pressure-assisted synthesis of NiTi. *Intermetallics*, **11,** 555-571.

Segal, V. M., 1995: Materials Processing by Simple Shear. *Mat Sci Eng a-Struct*, **197,** 157-164.

Segal, V. M., 1999: Equal channel angular extrusion: from macromechanics to structure formation. *Mat Sci Eng a-Struct*, **271,** 322-333.

Segal, V. M., 2004: Engineering and commercialization of equal channel angular extrusion (ECAE). *Mat Sci Eng a-Struct*, **386,** 269-276.

Wu, X., and I. W. Chen, 1992: Hot Extrusion of Ceramics. *Journal of the American Ceramic Society*, **75,** 1846-1853.